Developmental Cell, Vol. 9, 843–854, December, 2005, Copyright ©2005 by Elsevier Inc. DOI 10.1016/j.devcel.2005.11.006

Mitochondrial Regulation of Cell Cycle Progression during Development as Revealed by the *tenured* Mutation in *Drosophila*

Sudip Mandal,[1,2] Preeta Guptan,[1,2] Edward Owusu-Ansah,[1] and Utpal Banerjee[1,*]

[1] Department of Molecular, Cell, and Developmental Biology
Department of Biological Chemistry and Molecular Biology Institute
University of California, Los Angeles
Los Angeles, California 90095

Summary

The precise control of the cell cycle requires regulation by many intrinsic and extrinsic factors. Whether the metabolic status of the cell exerts a direct control over cell cycle checkpoints is not well understood. We isolated a mutation, *tenured* (*tend*), in a gene encoding cytochrome oxidase subunit Va. This mutation causes a drop in intracellular ATP to levels sufficient to maintain cell survival, growth, and differentiation, but not to enable progression through the cell cycle. Analysis of this gene in vivo and in cell lines shows that a specific pathway involving AMPK and p53 is activated that causes elimination of Cyclin E, resulting in cell cycle arrest. We demonstrate that in multiple tissues the mitochondrion has a direct and specific role in enforcing a G1-S cell cycle checkpoint during periods of energy deprivation.

Introduction

Cell cycle progression from one phase to the next is intricately controlled and is regulated by many checkpoints that respond to intrinsic and extrinsic signals. During the G1 phase, the cell integrates mitogenic and growth inhibitory signals and makes the decision to proceed, pause, or exit the cell cycle (Johnson and Walker, 1999). The core cell cycle machinery is composed of Cyclins and Cyclin-dependent kinases (CDKs), which are assembled and degraded during the course of cell division. Distinct Cyclins associate with and activate different CDKs throughout the cell cycle. For example, mammalian D-cyclins bind CDK4/6 to link external signals to the cell cycle and regulate progression through G1 (Weinberg, 1996). In contrast, *Drosophila* Cyclin D controls growth (Datar et al., 2000), whereas the G1-S transition is primarily controlled by Cyclin E (Richardson et al., 1993). *Drosophila* Cyclin E function requires it to bind to Cdc2c (similar to mammalian CDK2) in late G1. Later in the cell cycle, Cyclins A and B complex with CDK1 and are important for the G2-M transition; their subsequent degradation is critical for exit from mitosis.

The activity of Cyclin/CDK complexes is modulated by both activating and inhibitory phosphorylation of the CDK protein. The inhibitors INK4 and the CIP/KIP family of proteins are required for downregulation of the Cyclin/CDK complexes. In multicellular eukaryotes, stimuli including growth factors such as insulin (Bohni et al., 1999), TGFβ (Shi and Massague, 2003), Wnts (Nusse and Varmus, 1982), Hedgehog (reviewed by Ho and Scott, 2002), EGFR ligands (Lui and Grandis, 2002), and cell adhesion molecules (Lee and Juliano, 2004) can each act through signaling pathways to alter cell cycle progression. Similarly, environmental conditions such as nutrients and oxygen levels can also control the cell cycle (Carmeliet et al., 1998). In addition, intrinsic cellular components including oncogenes such as Myc (reviewed by Bouchard et al., 1998) and Ras (reviewed by Kerkhoff and Rapp, 1998), tumor suppressors like Tsc (Ito and Rubin, 1999; Potter et al., 2001; Tapon et al., 2001) and p53 (Vousden and Lu, 2002), microRNAs like bantam (Brennecke et al., 2003) and Sterile-20 kinases such as Slik (Hipfner and Cohen, 2003) and Hippo (Harvey et al., 2003; Udan et al., 2003; Wu et al., 2003) modulate the cell cycle.

The two components of the cell cycle, growth (increase in cell mass) and proliferation (increase in cell number), were initially viewed as aspects of a single process. However, molecular pathways controlling growth and proliferation can be separable. Mutations that block cell proliferation often do not block growth, while some cells can grow without dividing (reviewed in Edgar and Lehner, 1996; Schmelzle and Hall, 2000; Su and O'Farrell, 1998). The target of rapamycin protein (TOR) is an evolutionarily conserved serine/threonine kinase that has been shown to couple nutrients with growth factors (Shamji et al., 2003). Thus, TOR can be considered to act as a growth "rheostat" that helps in gauging nutrient levels and environmental stimuli, thereby regulating cell growth (Fingar and Blenis, 2004).

In early studies, Holley and Kiernan (1974) showed that low glucose levels can arrest 3T3 cells primarily in the G1 phase. Similarly, *Drosophila* cells arrest in interphase and metaphase when embryos are treated with cyanide, an inhibitor of oxidative phosphorylation, or when they are maintained under hypoxic conditions (DiGregorio et al., 2001). The mechanisms underlying these effects were poorly understood. In this paper, we show a link between mitochondrial function and the regulation of Cyclin E, and we provide evidence for a specific cell cycle checkpoint that senses the metabolic status of the cell.

Cellular energy is largely derived from the process of oxidative phosphorylation in the mitochondrion. The status of cellular energy stores is computed by AMP-activated protein kinase (AMPK). The heterotrimeric AMPK protein comprises a catalytic α subunit and regulatory β and γ subunits (Carling, 2004). AMP binds to the γ subunit of AMPK and allosterically promotes the phosphorylation of a critical threonine residue of AMPKα by AMPK kinase (Hawley et al., 1995). Cellular stresses that deplete ATP cause a rise in AMP levels, resulting in the activation of AMPK (Hardie, 2005). In a recent paper, Jones et al. (2005) showed that glucose limitation in mouse embryonic fibroblasts can cause phosphorylation of AMPK and activation of p53, a key mediator of

*Correspondence: banerjee@mbi.ucla.edu

[2] These authors contributed equally to this work.

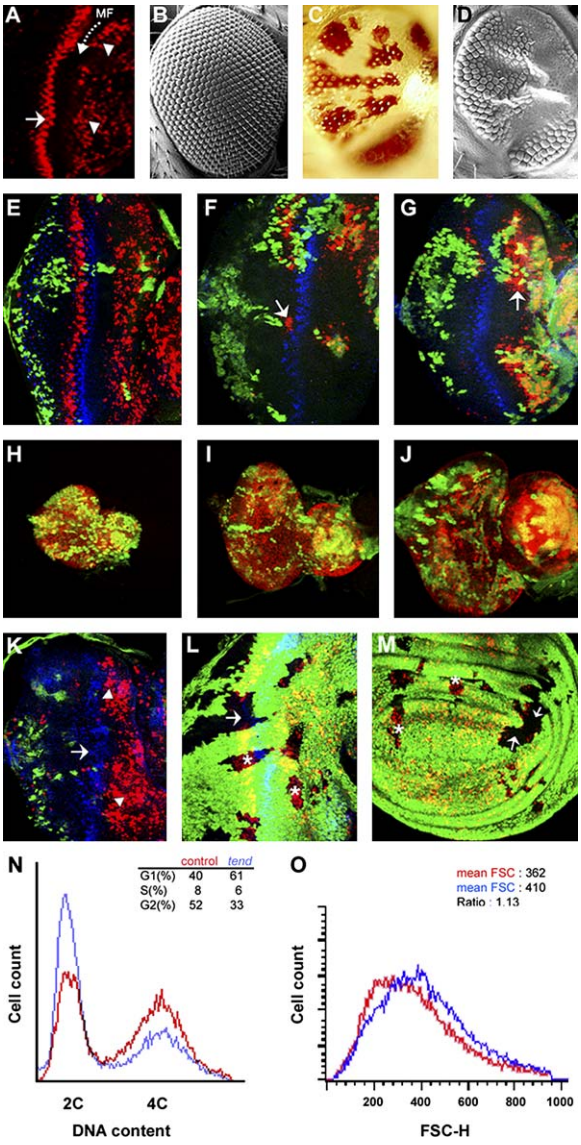

Figure 1. *tend* Larval and Adult Phenotypes

(A) BrdU incorporation (red) in a wild-type third instar larval eye imaginal disc. The dotted arrow marks the morphogenetic furrow (MF). Random BrdU incorporation is seen anterior to the MF (arrowheads). A single band of BrdU incorporation marking the initiation of the second mitotic wave is evident posterior to the furrow (arrow). BrdU was incorporated for 30 min; posterior is to the left.

(B–D) Eyes of adult flies. (B) Scanning electron micrograph (SEM) of a wild-type eye. (C) Somatic clones of *tend* shown in bright field. The mutant tissue is white and glossy, while wild-type tissue is red and faceted. (D) SEM of the same eye shown in (C). Facets are identifiable in the wild-type tissue, while the mutant tissue appears smooth due to lack of lenses. This phenotype is characteristic of loss of lens secreting cone and pigment cells that develop late and are derived from the cells that divide during the second mitotic wave.

(E–G) 30 min BrdU incorporation (red) in late third instar larval eye discs. Atonal (blue) marks the furrow. (E) In a control eye disc in which both green and non-green cells are wild-type, BrdU incorporation is normal (as in [A]). (F and G) In two examples in which the non-green tissue is $tend^{-}/tend^{-}$ and the green tissue is wild-type, BrdU incorporation is affected in the mutant tissue both anterior and posterior to the furrow. Some incorporation of BrdU in mutant tissue immediately adjacent to wild-type is indicated (arrows; see text for details). Posterior is to the left.

(H–J) BrdU incorporation (red) in early larval development in *tend* mutant clones (absence of green). In (H) second, (I) early third, and (J) mid third instar larval eye discs, extensive BrdU incorporation is evident in mutant clones.

(K) Prolonged (120 min) incorporation of BrdU in *tend* clones (absence of green). The furrow is marked with Armadillo (blue). Asynchronous BrdU incorporation anterior to the MF recovers in mutant tissue (arrowheads). However, cells fail to exit G1 arrest posterior to the furrow (arrow; compare BrdU [in red] with [E]).

(L–M) BrdU incorporation (red) is defective in *tend* clones (arrows) generated by *hsp70-flp* in (L) eye and in (M) wing imaginal discs of late third instar larvae. Small clones (asterisks) show normal BrdU incorporation (see text for details).

(N–O) Flow cytometric analysis of dissociated wing imaginal discs containing *tend* clones. Clones were generated by *hsp70-flp* 48 hr after egg deposition, and the discs were dissociated 72 hr thereafter. $tend^{-}/tend^{-}$ cells (non-green) are distinguishable in these assays from wild-type (GFP-positive and green). (N) A DNA profile of *tend* mutant cells (blue tracing), and that of wild-type cells (red tracing), indicates that a greater proportion of *tend* cells are in G1 (2C) compared to wild-type. (O) Cell size measured by flow cytometry. The wild-type population (in red) and the mutant population (in blue) are shown. Comparison of forward scatter count (FSC) values suggests that the mean size of mutant cells is approximately 13% larger than wild-type.

the cellular response to genotoxic stress and best known for its regulation of cell cycle checkpoints and apoptosis in response to irradiation (reviewed by Westphal, 1997).

In this paper, we report that mutations in several mitochondrial proteins cause a cell cycle arrest late during larval growth in *Drosophila*. We describe the mechanistic basis for this arrest for a mutation in *cytochrome oxidase Va*. Although it seems intuitive that energy levels should dictate the course of cell proliferation, the mechanism underlying this phenomenon was essentially unclear. It was also unclear if this process was simply due to the general slowdown of all cellular processes or whether it was due to the activation of a specific pathway in cell cycle regulation. In this paper, we describe how tissues in vivo respond to low ATP levels, through the activation of a Cyclin E-mediated cell cycle checkpoint leading to arrest in the G1 phase without affecting cellular differentiation and cell viability.

Results

Cell Cycle Progression Is Affected in *tenured* Mutant Clones

In the developing third instar wild-type eye disc, cell fate specification and patterning events sweep as a wave across the eye field, from the posterior to the anterior. The leading edge of the wave of differentiation is marked by an indentation, the morphogenetic furrow (MF). Two distinct phases of cell proliferation have been identified with respect to the furrow (Wolff and Ready, 1991). Anterior to the MF, BrdU incorporation is seen in randomly distributed cells (Figure 1A). This is followed by a G1 arrest of cells within the furrow, and a synchronous band of BrdU-positive cells can be seen immediately posterior to the furrow marking the initiation of the so-called second mitotic wave (SMW) (Figure 1A). In a *flp/FRT*-based mitotic recombination screen (Newsome et al., 2000), for mutations that give rise to a "glossy" adult eye phenotype (Figures 1B–1D), we identified a homozygous lethal mutation that causes a significant alteration in the BrdU incorporation pattern in the developing third

instar eye disc (Figures 1E–1G). Although large mutant clones are easily recoverable, implying that mutant cells have divided to generate them, mutant clones both anterior to the furrow and along the SMW fail to incorporate BrdU. The large clone size suggests that mutant cells must have divided earlier in development. Consistent with this notion, we found that BrdU incorporation is normal in homozygous mutant clones from late second instar and early third instar eye discs (Figures 1H–1J). In these experiments, BrdU was incorporated for 30 min. Upon prolonged BrdU incorporation, over 120 min, which allows for the detection of a slower entry into S phase (Tapon et al., 2001), BrdU incorporation is seen in mutant cells anterior to the furrow, but not along the SMW of third instar larval eye discs (Figure 1K). These results show that mutant cells can proliferate normally during the first several rounds of cell division in early larval instars, slow down their S phase later in the third instar, and eventually fail to enter S phase after G1 arrest in the MF. We termed this mutation *tenured* (*tend*).

The clones shown in Figures 1E–1K were generated with *ey-flp.* In this genetic background, the *flp* gene is expressed under the control of the *eyeless* (*ey*) enhancer, and the expressed Flp protein can potentially create recombination events and mutant clones in the eye throughout the early larval stages. Mutant clones were also generated in both eye and wing discs by using *hsp70-flp*, and *flp* was expressed only during the brief single heat pulse 48 hr after egg laying. BrdU incorporation is defective in such clones as well, both in eye and wing discs (Figures 1L and 1M), establishing that the cell cycle defect is not tissue specific. Wing discs containing clones were dissociated with trypsin to yield individual cells that were stained with Hoechst dye and analyzed by flow cytometry for cell cycle phasing. Compared with GFP-positive heterozygous cells, a greater fraction of $tend^{-}/tend^{-}$ cells are in the G1 phase of the cell cycle (Figure 1N). These findings in wing discs are consistent with the genetic results from the eye disc in which the mutant cells are held in G1. Furthermore, analysis of the average cell size, as gauged by forward scatter, shows that *tend* cells are about 13% larger than their wild-type neighbors (Figure 1O). These results indicate that, in *tend* clones, proliferation is affected without adversely affecting cell size.

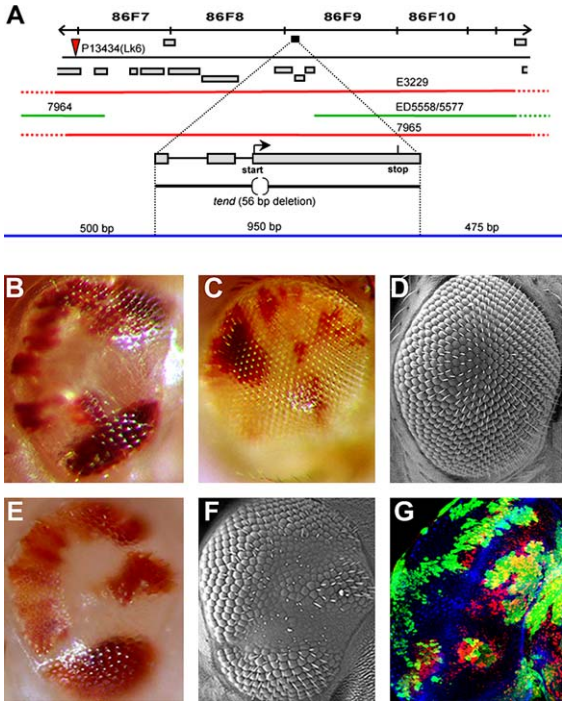

Figure 2. *tend* Is a Mutation in the Gene Encoding Subunit Va of Cytochrome c Oxidase

(A) Organization of genes (based on Flybase annotation) in the 86F7–86F10 region. The lethality of *tend* fails to complement lethality of flies deleted for the regions marked in red and complements those shown in green. By meiotic recombination, the eye phenotype was mapped to the right of P13434. The 56 bp deletion in *tend* is shown in relation to the translational start and stop sites. The genomic fragment used for transformation and rescue of the eye phenotype and lethality of *tend* is shown in blue.

(B–F) Eyes of adult flies. (B) Somatic clones of *tend* (white) appear smooth and glossy, and the wild-type tissue (red) shows normal facets. (C and D) $tend^{-}/tend^{-}$ clones were generated as in (B), but in a fly transformed with the genomic region shown as the blue line in (A). The mutant adult eye phenotype associated with *tend* is completely rescued, as seen in (C) bright field and (D) SEM images. (E and F) Somatic clones of *mRpL4* shown in (E) bright field and (F) SEM. The adult eye phenotype is similar to that seen for *tend* (compare with [B] and also Figures 1C and 1D).

(G) Third instar eye disc with clones of *mRpL4* (absence of green). The furrow is marked with Armadillo (blue). BrdU incorporation is defective in the clones both anterior and posterior to the MF, similar to that seen for *tend* (compare with Figures 1F and 1G).

Molecular Characterization of *tend*

The *tend* lethality was mapped by using deficiencies to the region between 86F6 and 86F9 on the right arm of the third chromosome (Figure 2A). The eye phenotype associated with this mutation was also independently mapped to this region by recombination mapping (see Experimental Procedures for details). Upon sequencing all of the ORFs in this region, we found a 56 base pair deletion in the gene encoding cytochrome c oxidase subunit Va (CoVa). CoVa is a small regulatory subunit of cytochrome c oxidase (Complex IV), which functions in the terminal step of the mitochondrial electron transport pathway. The 56 base pair deletion creates a null allele for the gene encoding CoVa; the resulting frame shift alters every functional amino acid and terminates prematurely within the mitochondrial leader sequence. The genomic region including the CoVa coding region and 500 bp each of upstream and downstream flanking DNA was used to generate transgenic flies. The lethality and eye phenotypes associated with the *tend* mutation were rescued in these transgenic flies (Figures 2B–2D). We conclude that *tend* represents a null allele for the gene encoding cytochrome c oxidase subunit Va (CoVa).

Somatic mutant clones of available recessive lethal mutations in additional mitochondrial genes were tested for their eye phenotype. Mutations in PdsW, a protein involved in the function of Complex I of the electron transport chain, and mitochondrial ribosomal proteins mRpL17 and mRpL4 give rise to a glossy eye phenotype similar to that seen for *tend* (example shown in Figures 2E and 2F). The similarity is also evident in eye disc clones in which BrdU incorporation is found to be defective (Figure 2G). Therefore, the transition from G1 to S phase of the cell cycle can be altered upon a reduction

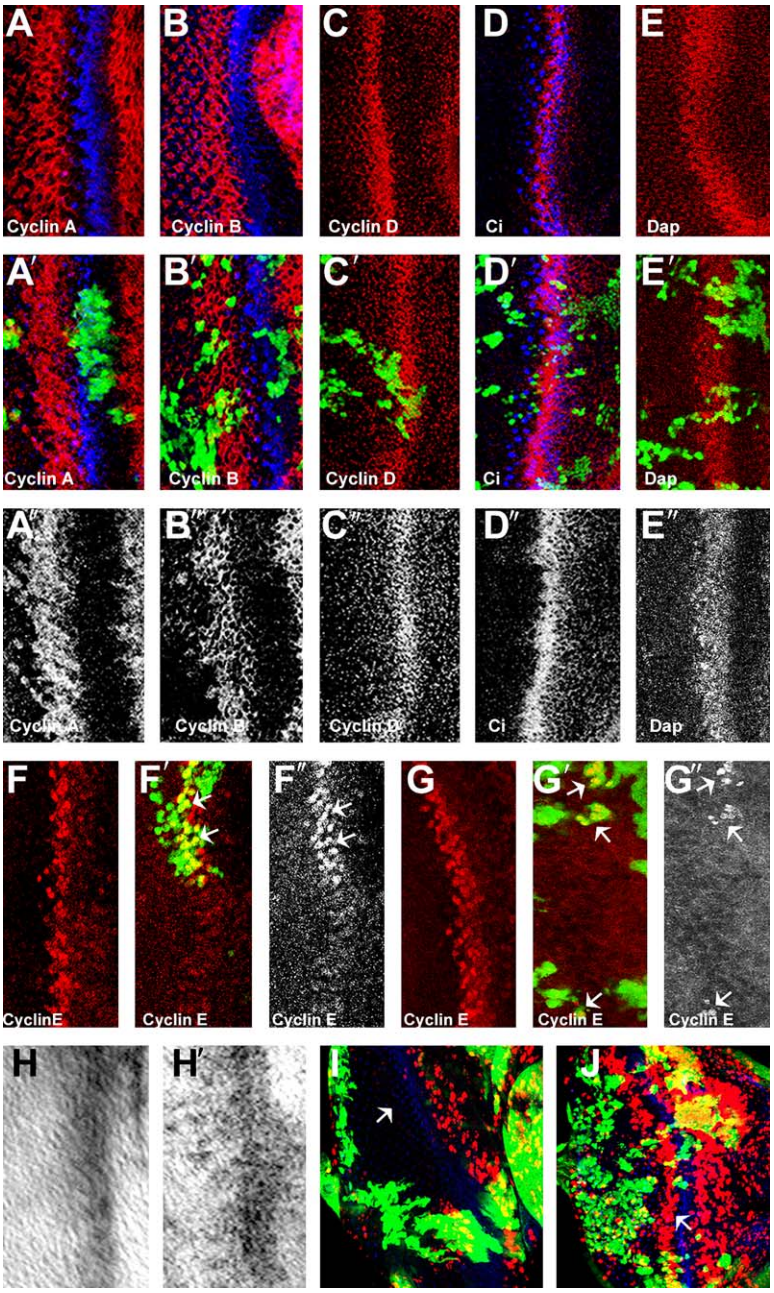

Figure 3. Specific Absence of Cyclin E Protein in *tend* Mutants

(A–G″) Expression of cell cycle regulators (red) in (A–G) wild-type and in (A′–G′) *tend* mutant clones shown as a merge (absence of green). For clarity, the red channel in (A′)–(G′) is also shown separately in grayscale in (A″)–(G″). All panels show the region adjacent to the furrow (marked in blue in [A]/[A′], [B]/[B′], and [D]/[D′]) of late third instar eye discs. Posterior is to the left. (A–A″) Cyclin A, (B–B″) Cyclin B, (C–C″) Cyclin D, (D–D″) Ci, and (E–E″) Dacapo are expressed normally in *tend* clones. (F and G) Wild-type expression of Cyclin E as a band posterior to the furrow by using independent antibodies against *Drosophila* Cyclin E raised in guinea pig and rat. (F′ and G′) Cyclin E expression is reduced in *tend* clones (absence of green). (F″ and G″) The red channel from (F′) and (G′) is shown again in grayscale for clarity. Arrows mark wild-type tissue that expresses Cyclin E.

(H and H′) Cyclin E RNA detected by in situ hybridization in eye discs. Posterior is to the left. (H) Cyclin E transcript in a wild-type eye disc. (H′) Cyclin E transcript is unaffected in a disc with clones of *tend*. Seven eye discs were analyzed under conditions under which independent staining showed that large mutant clones are present in every single disc (as shown in [F′] and [G′]).

(I and J) Rescue of BrdU incorporation in *tend* discs by overexpression of Cyclin E. (I) BrdU incorporation in sibling control discs that did not carry *hs-Cyclin E*. Third instar larvae were heat shocked for 90 min, followed by a 120 min recovery period. BrdU incorporation was then carried out for 120 min. Note that the band of incorporation behind the furrow is missing (marked by an arrow) in the clones, which is also described in Figure 1K. (J) BrdU incorporation was carried out after heat shock in *tend* discs carrying *hs-Cyclin E* as described for (I). The second mitotic wave of BrdU incorporation (marked by an arrow) recovers in mutant clones upon overexpression of Cyclin E.

of the mitochondrial function seen for mutations in one of several nuclear genes that encode mitochondrial proteins.

tend Mutant Cells Show a Marked Decrease in Cyclin E Protein Levels

To determine the molecular basis of the *tend* cell cycle defect, we analyzed the expression of Cyclins and Cyclin-associated proteins in mutant clones. Cyclin A and Cyclin B, essential for the G2-M transition, are expressed normally in *tend* mutant clones (Figures 3A–A″ and 3B–3B″). The expression of Cyclin D, one of the primary G1-cyclins is also unaffected (Figures 3C–C″). Likewise, the expression of Ci, a known inducer of Cyclin E expression (Duman-Scheel et al., 2002), is normal (Figures 3D–D″). No upregulation in the expression pattern of the only known *Drosophila* CDK inhibitor, Dacapo, is evident in the mutant clones (Figures 3E–E″). In contrast, the level of Cyclin E protein is considerably reduced in *tend* clones. Cyclin E expression in wild-type eye discs is seen as a narrow stripe immediately posterior to the MF (Figures 3F and 3G). In comparison, *tend* mutant cells show a significant reduction in Cyclin E protein. Two independently isolated antibodies against Cyclin E were used to confirm these results (Figures 3F′, 3F″, 3G′, and 3G″). Loss of Cyclin E expression in *tend* mutant clones is not regulated at the transcriptional level, as the Cyclin E transcript is expressed normally in mutant clones (Figures 3H and H′). Hence, the loss of Cyclin E in *tend* mutants is due to a decrease in Cyclin E protein translation, stability, or both. The G1-S block seen in the second mitotic wave in *tend* mutant clones is rescued

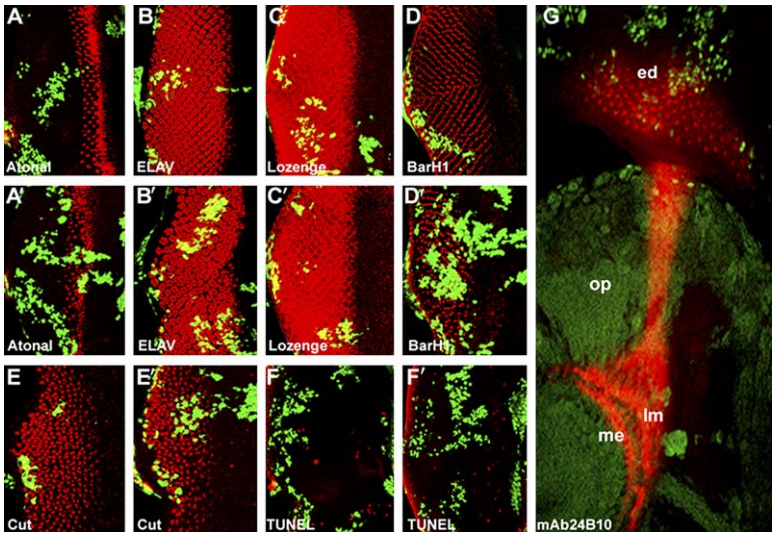

Figure 4. Patterning, Apoptosis, and Morphogenesis in *tend* Mutant Clones

(A–F′) Third instar larval eye discs with somatic clones (absence of green) stained with antibodies (red) against (A and A′) Atonal, (B and B′) ELAV, (C and C′) Lozenge, (D and D′) BarH1, (E and E′) Cut, or for (F and F′) TUNEL. In all cases, posterior is to the left. (A–F) Mock clones in which green and non-green tissue are both wild-type. (A′–F′) *tend* mutant clones are not green, while wild-type cells are green. Expression of Atonal, ELAV, Lozenge and BarH1, is normal in *tend* mutant clones, except for minor perturbations of the ordered array. Fewer Cut-positive cells are seen in the mutant tissue, and the number of TUNEL-positive cells is unaffected in the mutant.

(G) R cell axon projections in the optic lobe. mAb24B10 staining (red) was used to highlight cell bodies and axons of differentiating neurons. Cells within *tend* clones (absence of green) in the eye disc (ed) are capable of sending axonal projections into the lamina (lm) and medulla (me) of the optic lobe (op) in the brain.

upon overexpression of Cyclin E by using a *hsp70* driver (Figure 3J). This further demonstrates that the proliferation phenotype is due to the downregulation of Cyclin E in mutant clones.

Morphogenesis and Differentiation Are Largely Unaffected in *tend* Clones

Patterning events of differentiation and morphogenesis remain relatively normal in *tend* mutant clones (Figure 4). Photoreceptor (R) cell cluster formation is initiated with the expression of Atonal (Figures 4A and A′), and all differentiating neurons posterior to the furrow express ELAV (Figures 4B and B′). Only modest perturbation of spacing and orientation of the clusters is evident. The transcription factor Lozenge is also normally expressed in all undifferentiated mutant cells posterior to the furrow (Figures 4C and C′). Later recruitment of R1 and R6 cells is also normal, as evidenced by their expression of BarH1 (Figures 4D and D′). Importantly, *tend* mutant neurons not only express the neuronal markers, but they are also fully capable of undergoing major morphological changes such as extending their axonal projection to the optic center of the brain (Figure 4G). Cone cells expressing Cut are also seen (Figures 4E and E′), but their numbers are reduced, a likely contributing factor to the glossy adult eye phenotype. Finally, no change in numbers of TUNEL-positive cells is evident within the mutant clones, establishing that *tend* mutant cells do not show an increase in apoptosis in third instar mutant clones (Figures 4F and F′).

In conclusion, *tenured* cells are held in the G1 phase of the cell cycle, but they do not apoptose, can receive developmental signals, can differentiate into neuronal and nonneuronal cell types, and undergo major morphological changes such as extension of axons. With the notable exception of Cyclin E, expression of major cell cycle regulators also remains normal. We interpret these results to mean that the loss of mitochondrial function in the *tend* mutant does not cause a nonspecific blockage in all cellular functions; rather, it causes a specific block in cell cycle progression at the level of Cyclin E protein regulation.

tend Mutant Cells are Underrepresented

In order to generate the large $tend^{-}/tend^{-}$ mutant clones shown in Figure 1, we used the convenient *Minute* (*M*) genetic background. The $M^{+}tend^{-}$ cells are afforded an unfair growth advantage over their slow-growing $M^{-}tend^{+}$ neighbors. How would $tend^{-}/tend^{-}$ cells perform in their proliferation function when compared against cells that are completely wild-type? To address this issue, we generated *tend* mutant clones in a wild-type background and compared the number of cells in mutant clones ($tend^{-}/tend^{-}$) with their corresponding twin spots ($tend^{+}/tend^{+}$). Control clones generated with the wild-type parent FRT82B chromosome are indistinguishable in size from the corresponding twin spot irrespective of the size of the individual clones (Figure 5A). Analysis of $tend^{-}/tend^{-}$ clones and their wild-type twin spots revealed that they are similar in size when relatively small; however, as the clone size increases, the number of cells in a *tend* clone is far reduced compared to that in its sister twin spot (Figure 5B). The fact that the first few cell divisions in mutant clones of *tend* are normal is also consistent with the observation that small mutant clones of *tend* do not show the BrdU incorporation defect seen in large clones (marked by asterisks in Figures 1L and 1M). Thus, *tenured* cells can divide normally for 2–3 rounds of the cell cycle but then start to slow down, while their wild-type counterparts proceed through additional cell divisions. Newly derived mutant cells could have many more wild-type mitochondria or perdurant CoVa protein as compared to cells derived from later divisions. In fact, closer inspection of *ey-flp*-generated large clones shows BrdU-positive cells along the edges of the mutant tissue (Figures 1F and 1G). As *ey* is expressed continuously in the eye disc, one explanation for this apparent

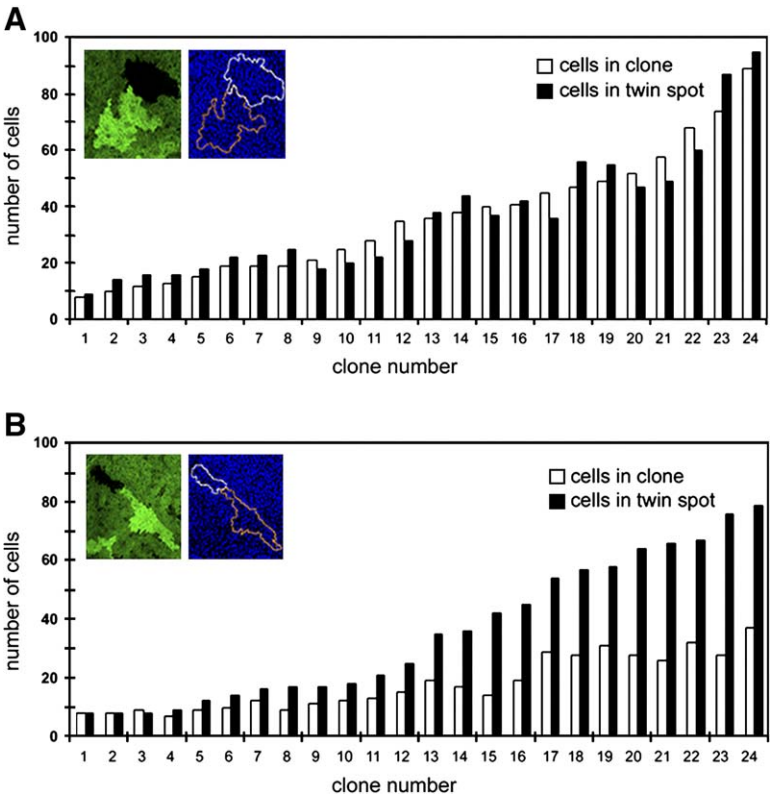

Figure 5. Dependence of the *tend* Phenotype on Clonal Cell Number

(A and B) The number of cells in mock wild-type (absence of green in the inset of [A]) or *tend* mutants (absence of green in the inset of [B]) were compared with their corresponding twin spots (bright green in the insets of [A] and [B]). Nuclei marked with To-pro-3 (blue) were counted to determine cell number. The results are displayed as histograms for 24 independently identified clones. (A) Clones of a wild-type parent chromosome (GFP^-/GFP^-, white bars) and their corresponding twin spots (GFP^+/GFP^+, black bars) are identical in size to one another irrespective of the number of cells in the clone. (B) Clones of $tend^-/tend^-$ cells (also GFP^-/GFP^-, white bars) compared with their corresponding twin spots (GFP^+/GFP^+, black bars). Small mutant clones are comparable in size to the wild-type twin spot, but large mutant clones are outcompeted by wild-type.

nonautonomy is that these mutant cells are recently derived in late divisions from the adjacent wild-type tissue. An alternate explanation of this apparent nonautonomy is that wild-type cells are able to rescue their mutant neighbors by a currently unknown mechanism. However, the first explanation is more likely since this effect is much reduced when clones are generated with *hsp70-flp* activated with a single pulse of heat shock (Figures 1L and 1M).

Proliferation in CoVa-Depleted Cells Correlates with Reduced Levels of ATP

To assess ATP levels in CoVa-depleted cells, *Drosophila* S2 cells were treated with *CoVa* dsRNA (Figure 6A) or with *GST* dsRNA (as an experimental control). The level of cellular ATP was measured in days after the dsRNA treatment. In Figure 6B, the ATP level in cells treated with *CoVa* dsRNA is normalized to that seen in *GST* dsRNA-treated cells. Two days after treatment, the cellular ATP level in *CoVa* dsRNA-treated cells is essentially identical to that in cells treated with *GST* dsRNA. Beginning on the third day, however, a gradual decrease in the ATP level is seen in *CoVa* dsRNA-treated cells, and it reaches a steady state of 43% of the control cells by the seventh day (Figure 6B).

Proliferation of *CoVa* dsRNA-treated cells correlates well with the gradual reduction of ATP (Figures 6C and 6D). On the first two days, *CoVa* dsRNA-treated cells grow on par with control cell populations. Thereafter, after an estimated four rounds of doubling, cells treated with *CoVa* dsRNA attenuate their rate of cell division and reach a plateau after the sixth day. The failure of the *CoVa* dsRNA-treated cells to undergo proliferation is due to significant reduction in the level of Cyclin E protein in these cells (Figure 6E). However, no reduction in the level of Cyclin E transcripts is found in *CoVa* dsRNA-treated cells (Figure 6F). The expression of the other G1-cyclin, Cyclin D, is also normal in these cells (Figure 6E). Trypan Blue staining confirmed that *CoVa* dsRNA-treated cells remain fully viable 8 days after treatment, when the final ATP and proliferation measurements are made. The number of cells that exclude Trypan Blue on the eighth day is similar for both *GST* dsRNA-treated cells (97.1% n = 1000) and cells treated with *CoVa* dsRNA (97.5% n = 1000). These observations are completely consistent with results from in vivo clones of *tend* mutant cells and show once again that the block in cell division is due to a specific regulation of the Cyclin E protein. Also, as for the in vivo results, these G1-arrested cells do not apoptose. Finally, the cell culture experiments provide a direct correlation between cellular ATP levels, proliferation, and CoVa function.

A Pathway for Cyclin E Control by ATP Levels

Previous studies have suggested that AMP-activated protein kinase (AMPK) can function as a sensor for cellular energy levels (reviewed by Hardie, 2004). We therefore measured total and phosphorylated (active) AMPK in *CoVa* dsRNA-treated cells. The level of phosphorylated AMPK rises as intracellular ATP drops in CoVa-depleted cells (Figure 6G). Therefore, loss of mitochondrial function and reduced ATP in S2 cells causes AMPK activation. The role of AMPK in this process was then tested in vivo. *Drosophila SNF4*γ encodes the AMP-sensing γ subunit of AMPK. Adult eyes of flies with clones of *SNF4*γ are wild-type (Figures 6H–6I′). The

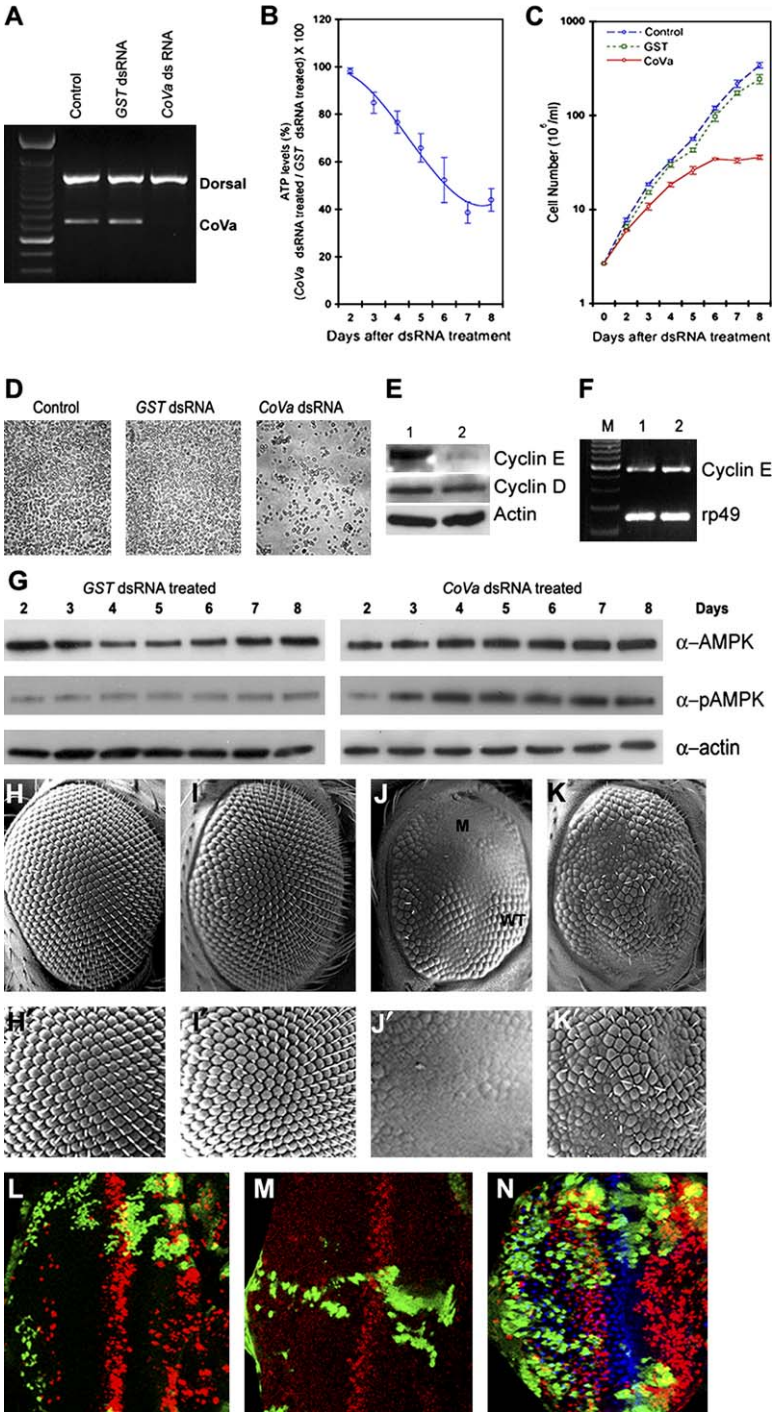

Figure 6. ATP Loss and AMPK Activation in Cells Depleted of CoVa

(A) S2 cells were treated with either *GST* or *CoVa* dsRNA, and the levels of *CoVa* and *dorsal* (as an unrelated control) transcripts were measured 2 days later by RT-PCR. Cells marked "Control" were not treated with any dsRNA. *CoVa* dsRNA causes a specific degradation of *CoVa* RNA.

(B) S2 cells were treated with *GST* (control) or *CoVa* dsRNA, and the cellular ATP level was measured by a luciferin-luciferase assay in the days after dsRNA treatment. The normalized ATP levels in *CoVa* dsRNA-treated cells as indicated along the ordinate are plotted as a function of days.

(C) Proliferation profile of untreated S2 cells (blue) and those treated with *GST* dsRNA (green) or *CoVa* dsRNA (red). After initial rounds of mitosis, *CoVa* dsRNA-treated cells slow down and stop dividing.

(D) S2 cells were either untreated (control) or treated with *GST* dsRNA or *CoVa* dsRNA as indicated. The cells shown were photographed 8 days after dsRNA treatment.

(E) Western blot analysis performed 7 days after treatment of S2 cells with *GST* dsRNA (lane 1) or *CoVa* dsRNA (lane 2) by using indicated antibodies. Cyclin D expression is comparable in both lanes, but Cyclin E is dramatically reduced in *CoVa* dsRNA-treated cells. Actin was used as a loading control.

(F) RT-PCR analysis of indicated transcripts 7 days after treatment of S2 cells with *GST* dsRNA (lane 1) or *CoVa* dsRNA (lane 2). Unlike the loss of Cyclin E protein seen in (E), *Cyclin E* RNA levels remain unchanged. rp49 was used as a control. M, marker lane.

(G) Western blot analysis of *GST* (control) or *CoVa* dsRNA-treated cells with antibodies against total (α-AMPK) and activated AMPK (α-pAMPK). In both control and experimental samples, the total AMPK level remains unchanged. However, pAMPK rises in *CoVa* dsRNA-treated cells, but not in the control. Actin was used as a loading control.

(H–K′) SEM of adult eyes. (H and H′) Wild-type facets shown in (H) low and (H′) high magnification. (I and I′) *SNF4*γ clones are wild-type. (J and J′) Clones of *tend* appear smooth. "WT" marks wild-type, and "M" marks mutant tissue shown in higher magnification in (J′). (K and K′) The smooth eye phenotype of *tend* clones is partially rescued in double mutant clones of *tend* and *SNF4*γ. The double mutant tissue is shown in higher magnification in (K′) (compare with [J′]).

(L) BrdU incorporation (red) in eye discs with double mutant clones of *tend* and *SNF4*γ (absence of green). A remarkable recovery of BrdU incorporation to virtually wild-type levels is seen in these clones (compare with Figures 1F and 1G).

(M) In double mutant clones of *tend* and *SNF4*γ, Cyclin E (red) expression recovers to wild-type levels.

(N) Normal BrdU incorporation (red) is seen in somatic clones of *dTOR* (absence of green).

tend mutation was recombined with the mutation in *SNF4*γ, and double mutant clones were generated in the eye. The adult eye of the double mutant for *tend* and *SNF4*γ contains many more facets (Figures 6K and 6K′) than is seen in *tend* mutant clones (Figures 6J and 6J′). Additionally, BrdU incorporation and Cyclin E expression is restored to normal in double mutant eye disc clones (Figures 6L and 6M). This implies that the

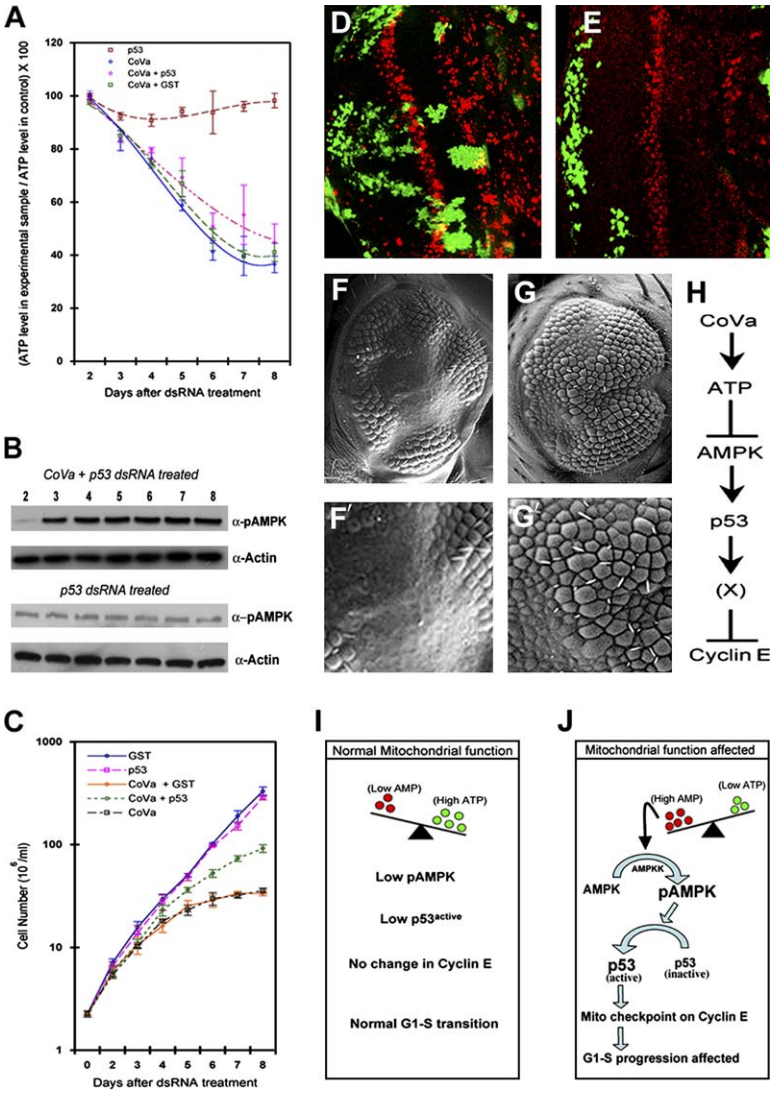

Figure 7. Function of p53 Downstream of AMPK

(A) S2 cells were either treated individually with *GST*, *p53*, and *CoVa* dsRNA or in combinations as indicated. Cellular ATP levels were assayed in the days after dsRNA treatment.

(B) Western blot analysis of *p53* dsRNA (control) or *CoVa* + *p53* dsRNA-treated cells with an antibody against activated AMPK (α-pAMPK). Actin was used as a loading control.

(C) Proliferation profile of S2 cells treated either with *GST* dsRNA, *p53* dsRNA, or *CoVa* dsRNA or in different combinations as indicated. In spite of the drop in ATP (shown in [A]) and the increase in p-AMPK (shown in [B]), the *CoVa* + *p53* dsRNA-treated cells show considerable rescue in their proliferation profile as compared with cells treated with *CoVa* dsRNA alone.

(D) BrdU incorporation (red) in the eye disc. Somatic clones doubly mutated for *tend* and *p53* (absence of green) show a rescue in BrdU incorporation compared with clones of *tend* alone (compare with Figures 1F and 1G).

(E) In eye discs with double mutant clones of *tend* and *p53*, Cyclin E (red) expression recovers to wild-type levels.

(F–G′) SEM of adult eyes. (F and F′) Clones of *tend* appear smooth. (G and G′) The smooth eye phenotype of *tend* clones is partially rescued in double mutant clones of *tend* and *p53*. Mutant clones are shown in higher magnification in (F′) and (G′) for comparison.

(H) The genetic pathway linking CoVa function to Cyclin E in the regulation of the G1-S transition during mitosis.

(I and J) A model for mitochondrial control of the Cyclin E-mediated mitotic checkpoint (see Discussion for details).

G1 checkpoint activated upon loss of CoVa can be overridden by the loss of AMPK, suggesting that AMPK acts downstream of *tend* to enforce the checkpoint. As an expected consequence of overriding a checkpoint, the immediate rescue of the BrdU phenotype and Cyclin E expression in the eye disc is more complete than the rescue of the adult eye phenotype.

Biochemical analysis in mammalian cell lines has identified two pathways: one mediated by TOR (Inoki et al., 2003), and the other mediated by p53 (Jones et al., 2005), downstream of AMPK. Activation of AMPK can lead to growth arrest by inhibiting TOR function (Inoki et al., 2003). However, cells in somatic clones of *dTOR* exhibit normal BrdU incorporation during larval eye development (Figure 6N). This indicates that inhibition of TOR primarily affects cell growth, but not cell proliferation, and is unlikely to be the target of AMPK in the pathway regulating Cyclin E described here.

Recent studies by Jones et al. (2005) have shown that high AMPK activity can also stabilize p53. We therefore compared ATP levels and proliferation profiles of cells doubly depleted for CoVa and p53 with those that are singly depleted for each. No significant decrease in cellular ATP is seen in S2 cells treated with *p53* dsRNA, and, as expected, cells treated with both *CoVa* and *p53* dsRNA show a profile of ATP reduction comparable to that seen for *CoVa* alone (Figure 7A). Furthermore, S2 cells doubly depleted for CoVa and p53 activate AMPK as in *CoVa* dsRNA-treated cells (Figure 7B). Remarkably, in spite of the low ATP levels and the consequent activation of AMPK, the p53 and CoVa doubly depleted cells proliferate significantly better than cells depleted for CoVa alone (Figure 7C). This suggests a role for p53 downstream of CoVa and AMPK in the control of the cell cycle. As in mammalian systems (Jones et al., 2005), it is likely that AMPK activates p53 posttranscriptionally, as we do not see a change in p53 RNA levels in CoVa-depleted cells (data not shown). The involvement of p53 in this pathway was then tested in vivo. *p53* mutant flies are homozygous viable and have wild-type eyes (Sogame et al., 2003). When *tend* clones are generated in flies that are otherwise homozygous mutant for *p53*, a remarkable rescue of the *tend* BrdU defect is observed in the eye disc (Figure 7D). The loss of Cyclin E expression is also rescued in the double mutant clones (Figure 7E). Additionally, the double mutant combination

shows a partial rescue of the glossy eye phenotype (Figures 7G and 7G′) associated with *tend* clones (Figures 7F and 7F′). This shows that the checkpoint activated in *tend* mutants can be overridden by mutations in p53, and it implicates p53 as the downstream effector of AMPK in controlling Cyclin E in this pathway. The genetic pathway linking mitochondrial function to Cyclin E is shown in Figure 7H.

Discussion

This study describes a mitotic checkpoint that is activated in periods of lowered mitochondrial function (Figures 7I and 7J). We show that a null mutation in *CoVa*, a nuclear-encoded component of the mitochondrial electron transport chain, lowers intracellular ATP to about 40% of normal. This ATP level is sufficient to support cell survival, growth, and differentiation, and it allows us to genetically dissect the pathway connecting mitochondrial function to cell division. The 60% reduction in ATP levels in mutant cells activates the energy sensor AMPK, presumably due to an increase in cellular AMP levels. In turn, AMPK activates the cell cycle checkpoint regulator p53 and brings about a cell cycle arrest by reducing levels of the rate-limiting protein Cyclin E. Although it might be assumed that mutations in mitochondrial proteins would cause a general slowdown of all cellular processes, our results show that *tend* mutant cells are remarkably healthy and are capable of differentiation and morphogenesis. In the eye disc, *tend* mutant cells adopt their appropriate fate, transcribe genes related to proliferation and differentiation control, and are capable of extensive morphological changes, such as projecting axons to their target regions in the brain. The only cellular dysfunction that we have detected upon the 60% drop in ATP levels in *tend* mutants is the block in cell cycle. Furthermore, we did not observe any increase in apoptosis in *tend* mutant cells, although it is likely that other mitochondrial mutations that cause a more precipitous drop in ATP levels would activate cell death mechanisms. We conclude that a mechanism involving Cyclin E operates to block the cell cycle specifically at the G1-S transition point in response to a limiting threshold in its ATP level (Figures 7I and 7J).

Cell division is an energy-intensive process, and inhibition of the cell cycle by an ATP-dependent checkpoint is critical. Checkpoints are surveillance mechanisms that respond to stress and activate processes that maintain viability. AMPK and p53 are not required for regulating cell cycle progression under normal growth conditions in wild-type flies. As a result, loss-of-function mutations in either AMPKγ or p53 have a wild-type eye phenotype. However, AMPK and p53 do function to control the cell cycle in response to low ATP by triggering downregulation of Cyclin E protein. As has been described for other checkpoints, we were able to override this cell cycle arrest. This was achieved by making double mutant clones of *tend* and *p53* or *tend* and *AMPK*γ. The result is a dramatic rescue of the BrdU incorporation phenotype as well as Cyclin E expression in the double mutant cells. Previous work has shown *Drosophila* p53 to have a role in irradiation-mediated cell death (Brodsky et al., 2000; Sogame et al., 2003). In contrast, mammalian p53 has been shown to have a function in both cell cycle and apoptosis. We demonstrate that *Drosophila* p53 also functions in cell cycle arrest under conditions of modest loss of metabolic function. It is likely that the triggering of apoptotic pathways by irradiation requires a higher threshold of p53 function. This notion is consistent with work in mammalian systems in which small changes in p53 levels or activity trigger a cell cycle arrest. Moreover, as the levels increase the cells turn on the apoptotic machinery (Vousden, 2000).

In addition to CoVa, we found that mutations in several other mitochondrial proteins, primarily large and small subunits of ribosomal proteins (mRpLs and mRpSs), also show a BrdU incorporation block similar to that seen in *tend*. While the details of the molecular pathways affected in these other mutants remain to be investigated, it is likely that these mutations affect the translation of proteins encoded by the mitochondrial genome and as a result prevent the electron transport chain from functioning optimally. Since multiple genes encode proteins of the ribosomal subunits, their functions may be redundant, and a mutation in any one component may only partially reduce mitochondrial translation. However, not all mRp mutations show cell cycle arrest (Frei et al., 2005; Galloni, 2003). We speculate that when mutations are made in each mitochondrial protein and in combinations, it will be possible to identify mechanisms that create a balance between cell proliferation, cell growth, and cell death. Our in vivo observations of deprivation of mitochondrial function are similar to the observations made in cell culture experiments in which mouse embryonic fibroblasts are exposed to different levels of glucose (Jones et al., 2005). Whereas cells completely deprived of glucose die, cells receiving 0.5 mM glucose show a p53-dependent cell cycle arrest similar to that seen upon partial ATP deprivation in our studies.

The downregulation of Cyclin E in response to mitochondrial dysfunction is posttranscriptional. It is not yet clear whether this is due to reduced translation of the Cyclin E transcript or accelerated degradation of the Cyclin E protein. In *S. cerevisiae*, Cln3, a Cyclin critical for the G1-S transition, is regulated at the translational level in response to the absence of a fermentable carbon source (Polymenis and Schmidt, 1997). A similar mechanism could potentially provide a means of altering Cyclin E protein levels without affecting other protein products in the cell. On the other hand, several Ubiquitin ligases, including Archipelago, Sina, and Ebi (Boulton et al., 2000; Brumby et al., 2004; Moberg et al., 2001), have been associated with normal Cyclin E degradation during the cell cycle. However, in preliminary studies of the kind that allowed us to identify *AMPK* and *p53* as downstream components of *tend*, we were unable to detect a role for *archipelago*, *sina*, or *ebi* in this process. This is not surprising since the *Drosophila* genome has over 50 potential genes encoding members of the E3 Ubiquitin ligase complex (Ou et al., 2003). Finally, in mammalian systems, p53-activated G1-S arrest involves transcriptional activation of the CDK inhibitor p21 (el-Deiry et al., 1993). The only known homolog of the p27/p21 family of proteins in *Drosophila* is Dacapo, which is not upregulated in *tend* mutant cells. Although, no other p21-like gene has been identified, it remains a possibility that a protein with low homology to p21 is

involved as a CDK inhibitor. In Figure 7, we have designated the missing component between p53 and Cyclin E as X. Given the tools available in *Drosophila*, future modifier screens should reveal the identity of X.

An interesting finding from this work is that *tend* cells are not compromised in their size. In fact, mutant cells show a slight (13%) increase in size compared to their wild-type counterparts. Previous work has shown that AMPK activation inhibits TOR function, and it was therefore conceivable that the cell cycle arrest phenotype in *tend* could be a consequence of a similar growth arrest. Instead, our study shows that *tend* mutants have a phenotype complementary to that of *TOR*. Cells mutant for *TOR* are smaller in size and show normal BrdU incorporation, while *tend* cells are slightly larger than wild-type and are affected in the G1-S transition step of cell division.

This study is an in vivo demonstration of a mitochondrial regulation of a checkpoint blocking cell cycle progression. Activation of this regulatory mechanism to block the cell cycle will allow a cell to weather a period of energy deprivation by pausing in the cell cycle and resuming proliferation upon the return of energy sources. Periods of energy insufficiency can be due to a variety of reasons, including limited oxygen availability. Hypoxia diminishes the cell's oxidative phosphorylation capacity and can cause cell cycle arrest in a number of species, including *Drosophila* (DiGregorio et al., 2001) and *C. elegans* (Padilla et al., 2002). Similarly, it has been suggested that the ability of cells deep inside solid tumors to withstand radiation as well as chemotherapy is due to hypoxia-induced G1 arrest (Graeber et al., 1994; Kim et al., 1997). It is tempting to speculate that cells could use this mode of cell cycle arrest to their advantage during normal development. Hematopoetic stem cells in the bone marrow are distributed along a gradient of oxygen; stem cells residing in more hypoxic conditions cycle slowly, while proliferating progenitor cells are in normoxic regions (Danet et al., 2003). It will be interesting to determine in future studies if the cell cycle arrest observed in stem cells utilizes pathways that we have described here for CoVa.

Experimental Procedures

Stocks and Mutations

y w ey-flp; FRT82B males were mutagenized with 25 mM ethylmethanesulfonate (EMS) and crossed to *y w ey-flp; FRT82B P[w$^+$]cl-R3/TM6B Tb, y$^+$*. Similar in function to a *Minute cl-R3* is a cell-lethal mutation (Newsome et al., 2000). Mosaic-eyed flies with an eye phenotype were crossed to balancer lines and maintained as stocks. *p53$^{11\text{-}1B\text{-}1}$*, *P[SUP]SNF4A$\gamma^{KG00325}$*, *P[w$^+$]mRpL4[k14608]*, *P[SUP]mRpL17[KG06809]*, *P[w$^+$]Pdsw[k10101]*, and *TOR[DeltaP] FRT40A* were all from the Bloomington Stock Center. *hs-cyclinEII* flies were a gift from Helena Richardson.

Molecular Mapping

To map the *tend* eye phenotype, we recombined a distal P element, P[SUP]KG03257, at 87A4 onto the FRT chromosome carrying the *tend* mutation by using standard meiotic recombination procedures. The presence of *tend* and P[SUP]KG03257 was determined by crossing with *y w ey-flp; FRT82B P[w$^+$]cl-R3/TM6B Tb, y$^+$* and scoring for the glossy eye phenotype. P[SUP]KG03257 carries a *y$^+$* marker, and the presence of the P element was determined by the gray body color in an otherwise yellow background. The *FRT82B tend, P[SUP]KG03257* recombined chromosome was placed in *trans* with the P element, P[GT1]BG01876, on 86F5. Recombinants between the two P elements were isolated as white-eyed flies in an otherwise red-eyed population. Again, the presence and absence of *tend* was determined by making adult clones. The site of recombination was mapped to an interval between SNPs that marked the recombinant chromosome. Based on the location of the SNPs, the map position of the phenotype was further refined to a region between 86F6 and 86F9.

Generation of Clones, Immunohistochemistry, and FACS

Adult eye clones were made by using flies of the genotype *y w ey-flp; FRT82B P[w$^+$]cl-R3/TM6B Tb, y$^+$*. Mutant clones were marked by the absence of pigmentation.

Larval clones were generated by using *y w ey-flp; FRT82B Ubi-GFP RpS3/TM6B Tb, y$^+$* or *hsp70-flp; FRT82B Ubi-GFP RpS3/TM6B Tb, y$^+$*. Large clones that gave mutant cells a growth advantage were made possible because of the ribosomal mutations *Rps3* or *M* on the wild-type chromosome. For the experiment shown in Figure 5, clones were made with *hsp70-flp; FRT82B Ubi-GFP/TM6B Tb, y$^+$*.

The following antibodies were used: rat anti-BrdU (Abcam), rabbit anti-Atonal (Y.N. Jan), rabbit anti-BarH1 (T. Kojima), guinea pig anti-Cyclin E (T. Orr-Weaver), rat anti-Cyclin E and mouse anti-Cyclin E (H. Richardson), mouse anti-Cyclin D (W. Du), mouse anti-Dacapo (I. Hariharan), rat anti-Ci (R. Holmgren), mouse anti-GFP and rabbit anti-GFP (Molecular Probes), rabbit anti-phospho-AMPKα (Thr-172, 40H9) and rabbit anti-AMPKα (Cell Signaling), rat anti-elav, mAb24B10, mouse anti-Cyclin A, mouse anti-Cyclin B, mouse anti-Armadillo, mouse anti-Actin, mouse anti-Cut (Iowa Hybridoma Center), and mouse anti-Lozenge (Lebestky et al., 2000).

Imaginal disc BrdU incorporation was carried out for 30 min or 2 hr as described (de Nooij and Hariharan, 1995). Apoptotic cells were identified by TUNEL labeling with an in situ cell death detection kit (Roche).

Flow cytometric analysis was carried out as described (Neufeld et al., 1998) on wing disc cells dispersed with Trypsin, stained with Hoechst 33342 dye (Sigma), and sorted by using a Becton Dickinson FACS Calibur Analytic Flow Cytometer.

Cell Culture, RNAi, and ATP Assay

To prepare dsRNA 500 bp of coding sequence for CoVa, p53, or GST was PCR amplified with primers carrying a 5′ T7 RNA polymerase binding site. dsRNA was purified by using a Megascript RNAi kit (Ambion) and was stored at −20ºC. Cells were treated with 20 μg dsRNA individually or 20 μg each in combination. S2 cells seeded to a density of 10^6 per well in 6-well plates were treated on the following day with dsRNA as described (Clemens et al., 2000). The day of dsRNA treatment is termed Day 0. The cells were split and reseeded to a density of 10^6 on Day 2 and Day 5 after dsRNA treatment. Cells were isolated each day from Day 2 to Day 8 for ATP, protein, and RNA measurements. ATP measurements were carried out by using a luciferin-luciferase-based ATP Assay kit (Calbiochem) and were normalized to the cell number.

Acknowledgments

We thank Vivian Liao and Kha Nguyen for their help with several experiments and Kevin Griffin, Cory Evans, Volker Hartenstein, Larry Zipursky, and members of the Banerjee laboratory for critical review of the manuscript. We thank Y.N. Jan, T. Kojima, T. Orr-Weaver, H. Richardson, W. Du, I. Hariharan, R. Holmgren, and the Iowa Hybridoma Center for antibodies and B. Dickson and the Bloomington Stock Center for fly stocks. We thank Girish Ratnaparkhi and Albert Courey for their help with cell-line experiments. We are indebted to Gerald Call and members of the UCLA undergraduate consortium for characterizing mitochondrial ribosomal mutations. We acknowledge the Jonsson Comprehensive Cancer Center FACS analysis core for their help in cell sorting. This study was supported by National Institutes of Health grant R01-EY08152 to U.B.

Received: August 25, 2005
Revised: November 2, 2005
Accepted: November 10, 2005
Published: December 5, 2005

References

Bohni, R., Riesgo-Escovar, J., Oldham, S., Brogiolo, W., Stocker, H., Andruss, B.F., Beckingham, K., and Hafen, E. (1999). Autonomous control of cell and organ size by CHICO, a *Drosophila* homolog of vertebrate IRS1–4. Cell *97*, 865–875.

Bouchard, C., Staller, P., and Eilers, M. (1998). Control of cell proliferation by Myc. Trends Cell Biol. *8*, 202–206.

Boulton, S.J., Brook, A., Staehling-Hampton, K., Heitzler, P., and Dyson, N. (2000). A role for Ebi in neuronal cell cycle control. EMBO J. *19*, 5376–5386.

Brennecke, J., Hipfner, D.R., Stark, A., Russell, R.B., and Cohen, S.M. (2003). *bantam* encodes a developmentally regulated microRNA that controls cell proliferation and regulates the proapoptotic gene *hid* in *Drosophila*. Cell *113*, 25–36.

Brodsky, M.H., Nordstrom, W., Tsang, G., Kwan, E., Rubin, G.M., and Abrams, J.M. (2000). *Drosophila* p53 binds a damage response element at the reaper locus. Cell *101*, 103–113.

Brumby, A., Secombe, J., Horsfield, J., Coombe, M., Amin, N., Coates, D., Saint, R., and Richardson, H. (2004). A genetic screen for dominant modifiers of a cyclin E hypomorphic mutation identifies novel regulators of S-phase entry in *Drosophila*. Genetics *168*, 227–251.

Carling, D. (2004). The AMP-activated protein kinase cascade—a unifying system for energy control. Trends Biochem. Sci. *29*, 18–24.

Carmeliet, P., Dor, Y., Herbert, J.M., Fukumura, D., Brusselmans, K., Dewerchin, M., Neeman, M., Bono, F., Abramovitch, R., Maxwell, P., et al. (1998). Role of HIF-1α in hypoxia-mediated apoptosis, cell proliferation and tumour angiogenesis. Nature *394*, 485–490.

Clemens, J.C., Worby, C.A., Simonson-Leff, N., Muda, M., Maehama, T., Hemmings, B.A., and Dixon, J.E. (2000). Use of double-stranded RNA interference in *Drosophila* cell lines to dissect signal transduction pathways. Proc. Natl. Acad. Sci. USA *97*, 6499–6503.

Danet, G.H., Pan, Y., Luongo, J.L., Bonnet, D.A., and Simon, M.C. (2003). Expansion of human SCID-repopulating cells under hypoxic conditions. J. Clin. Invest. *112*, 126–135.

Datar, S.A., Jacobs, H.W., de la Cruz, A.F., Lehner, C.F., and Edgar, B.A. (2000). The *Drosophila* cyclin D-Cdk4 complex promotes cellular growth. EMBO J. *19*, 4543–4554.

de Nooij, J.C., and Hariharan, I.K. (1995). Uncoupling cell fate determination from patterned cell division in the *Drosophila* eye. Science *270*, 983–985.

DiGregorio, P.J., Ubersax, J.A., and O'Farrell, P.H. (2001). Hypoxia and nitric oxide induce a rapid, reversible cell cycle arrest of the *Drosophila* syncytial divisions. J. Biol. Chem. *276*, 1930–1937.

Duman-Scheel, M., Weng, L., Xin, S., and Du, W. (2002). Hedgehog regulates cell growth and proliferation by inducing Cyclin D and Cyclin E. Nature *417*, 299–304.

Edgar, B.A., and Lehner, C.F. (1996). Developmental control of cell cycle regulators: a fly's perspective. Science *274*, 1646–1652.

el-Deiry, W.S., Tokino, T., Velculescu, V.E., Levy, D.B., Parsons, R., Trent, J.M., Lin, D., Mercer, W.E., Kinzler, K.W., and Vogelstein, B. (1993). WAF1, a potential mediator of p53 tumor suppression. Cell *75*, 817–825.

Fingar, D.C., and Blenis, J. (2004). Target of rapamycin (TOR): an integrator of nutrient and growth factor signals and coordinator of cell growth and cell cycle progression. Oncogene *23*, 3151–3171.

Frei, C., Galloni, M., Hafen, E., and Edgar, B.A. (2005). The *Drosophila* mitochondrial ribosomal protein mRpL12 is required for Cyclin D/Cdk4-driven growth. EMBO J. *24*, 623–634.

Galloni, M. (2003). Bonsai, a ribosomal protein S15 homolog, involved in gut mitochondrial activity and systemic growth. Dev. Biol. *264*, 482–494.

Graeber, T.G., Peterson, J.F., Tsai, M., Monica, K., Fornace, A.J., Jr., and Giaccia, A.J. (1994). Hypoxia induces accumulation of p53 protein, but activation of a G1-phase checkpoint by low-oxygen conditions is independent of p53 status. Mol. Cell. Biol. *14*, 6264–6277.

Hardie, D.G. (2004). The AMP-activated protein kinase pathway—new players upstream and downstream. J. Cell Sci. *117*, 5479–5487.

Hardie, D.G. (2005). New roles for the LKB1 →AMPK pathway. Curr. Opin. Cell Biol. *17*, 167–173.

Harvey, K.F., Pfleger, C.M., and Hariharan, I.K. (2003). The *Drosophila* Mst ortholog, hippo, restricts growth and cell proliferation and promotes apoptosis. Cell *114*, 457–467.

Hawley, S.A., Selbert, M.A., Goldstein, E.G., Edelman, A.M., Carling, D., and Hardie, D.G. (1995). 5′-AMP activates the AMP-activated protein kinase cascade, and Ca2+/calmodulin activates the calmodulin-dependent protein kinase I cascade, via three independent mechanisms. J. Biol. Chem. *270*, 27186–27191.

Hipfner, D.R., and Cohen, S.M. (2003). The *Drosophila* sterile-20 kinase slik controls cell proliferation and apoptosis during imaginal disc development. PLoS Biol. *1*, E35.

Ho, K.S., and Scott, M.P. (2002). Sonic hedgehog in the nervous system: functions, modifications and mechanisms. Curr. Opin. Neurobiol. *12*, 57–63.

Holley, R.W., and Kiernan, J.A. (1974). Control of the initiation of DNA synthesis in 3T3 cells: low-molecular weight nutrients. Proc. Natl. Acad. Sci. USA *71*, 2942–2945.

Inoki, K., Zhu, T., and Guan, K.L. (2003). TSC2 mediates cellular energy response to control cell growth and survival. Cell *115*, 577–590.

Ito, N., and Rubin, G.M. (1999). gigas, a *Drosophila* homolog of tuberous sclerosis gene product-2, regulates the cell cycle. Cell *96*, 529–539.

Johnson, D.G., and Walker, C.L. (1999). Cyclins and cell cycle checkpoints. Annu. Rev. Pharmacol. Toxicol. *39*, 295–312.

Jones, R.G., Plas, D.R., Kubek, S., Buzzai, M., Mu, J., Xu, Y., Birnbaum, M.J., and Thompson, C.B. (2005). AMP-activated protein kinase induces a p53-dependent metabolic checkpoint. Mol. Cell *18*, 283–293.

Kerkhoff, E., and Rapp, U.R. (1998). Cell cycle targets of Ras/Raf signalling. Oncogene *17*, 1457–1462.

Kim, C.Y., Tsai, M.H., Osmanian, C., Graeber, T.G., Lee, J.E., Giffard, R.G., DiPaolo, J.A., Peehl, D.M., and Giaccia, A.J. (1997). Selection of human cervical epithelial cells that possess reduced apoptotic potential to low-oxygen conditions. Cancer Res. *57*, 4200–4204.

Lebestky, T., Chang, T., Hartenstein, V., and Banerjee, U. (2000). Specification of *Drosophila* hematopoietic lineage by conserved transcription factors. Science *288*, 146–149.

Lee, J.W., and Juliano, R. (2004). Mitogenic signal transduction by integrin- and growth factor receptor-mediated pathways. Mol. Cells *17*, 188–202.

Lui, V.W., and Grandis, J.R. (2002). EGFR-mediated cell cycle regulation. Anticancer Res. *22*, 1–11.

Moberg, K.H., Bell, D.W., Wahrer, D.C., Haber, D.A., and Hariharan, I.K. (2001). Archipelago regulates Cyclin E levels in *Drosophila* and is mutated in human cancer cell lines. Nature *413*, 311–316.

Neufeld, T.P., de la Cruz, A.F., Johnston, L.A., and Edgar, B.A. (1998). Coordination of growth and cell division in the *Drosophila* wing. Cell *93*, 1183–1193.

Newsome, T.B., Asling, B., and Dickson, B.J. (2000). Analysis of *Drosophila* photoreceptor axon guidance in eye-specific mosaics. Development *127*, 851–860.

Nusse, R., and Varmus, H.E. (1982). Many tumors induced by the mouse mammary tumor virus contain a provirus integrated in the same region of the host genome. Cell *31*, 99–109.

Ou, C.Y., Pi, H., and Chien, C.T. (2003). Control of protein degradation by E3 ubiquitin ligases in *Drosophila* eye development. Trends Genet. *19*, 382–389.

Padilla, P.A., Nystul, T.G., Zager, R.A., Johnson, A.C., and Roth, M.B. (2002). Dephosphorylation of cell cycle-regulated proteins correlates with anoxia-induced suspended animation in *Caenorhabditis elegans*. Mol. Biol. Cell *13*, 1473–1483.

Polymenis, M., and Schmidt, E.V. (1997). Coupling of cell division to cell growth by translational control of the G1 cyclin CLN3 in yeast. Genes Dev. *11*, 2522–2531.

Potter, C.J., Huang, H., and Xu, T. (2001). *Drosophila* Tsc1 functions with Tsc2 to antagonize insulin signaling in regulating cell growth, cell proliferation, and organ size. Cell *105*, 357–368.

Richardson, H.E., O'Keefe, L.V., Reed, S.I., and Saint, R. (1993). A *Drosophila* G1-specific cyclin E homolog exhibits different modes of expression during embryogenesis. Development *119*, 673–690.

Schmelzle, T., and Hall, M.N. (2000). TOR, a central controller of cell growth. Cell *103*, 253–262.

Shamji, A.F., Nghiem, P., and Schreiber, S.L. (2003). Integration of growth factor and nutrient signaling: implications for cancer biology. Mol. Cell *12*, 271–280.

Shi, Y., and Massague, J. (2003). Mechanisms of TGF-β signaling from cell membrane to the nucleus. Cell *113*, 685–700.

Sogame, N., Kim, M., and Abrams, J.M. (2003). *Drosophila* p53 preserves genomic stability by regulating cell death. Proc. Natl. Acad. Sci. USA *100*, 4696–4701.

Su, T.T., and O'Farrell, P.H. (1998). Size control: cell proliferation does not equal growth. Curr. Biol. *8*, R687–R689.

Tapon, N., Ito, N., Dickson, B.J., Treisman, J.E., and Hariharan, I.K. (2001). The *Drosophila* tuberous sclerosis complex gene homologs restrict cell growth and cell proliferation. Cell *105*, 345–355.

Udan, R.S., Kango-Singh, M., Nolo, R., Tao, C., and Halder, G. (2003). Hippo promotes proliferation arrest and apoptosis in the Salvador/Warts pathway. Nat. Cell Biol. *5*, 914–920.

Vousden, K.H. (2000). p53: death star. Cell *103*, 691–694.

Vousden, K.H., and Lu, X. (2002). Live or let die: the cell's response to p53. Nat. Rev. Cancer *2*, 594–604.

Weinberg, R.A. (1996). E2F and cell proliferation: a world turned upside down. Cell *85*, 457–459.

Westphal, C.H. (1997). Cell-cycle signaling: Atm displays its many talents. Curr. Biol. *7*, R789–R792.

Wolff, T., and Ready, D.F. (1991). The beginning of pattern formation in the *Drosophila* compound eye: the morphogenetic furrow and the second mitotic wave. Development *113*, 841–850.

Wu, S., Huang, J., Dong, J., and Pan, D. (2003). hippo encodes a Ste-20 family protein kinase that restricts cell proliferation and promotes apoptosis in conjunction with salvador and warts. Cell *114*, 445–456.